ELSEVIER

Journal of Alloys and Compounds 317–318 (2001) 237–244

Journal of ALLOYS AND COMPOUNDS

www.elsevier.com/locate/jallcom

Layered ternary transition metal nitrides; synthesis, structure and physical properties

Duncan H. Gregory[a,*], Paul M. O'Meara[a], Alexandra G. Gordon[a], Daniel J. Siddons[a], Alexander J. Blake[a], Marten G. Barker[a], Thomas A. Hamor[b], Peter P. Edwards[b]

[a]*School of Chemistry, University of Nottingham, Nottingham NG7 2RD, UK*
[b]*School of Chemistry, University of Birmingham, Edgbaston, Birmingham B15 2TT, UK*

Abstract

Two-dimensional structures are an emerging class of materials within nitride chemistry. We report here our systematic studies of two groups of these layered compounds: **1** Lithium transition metal compounds, $Li_{3-x-y}\square_yM_xN$ (M=Co, Ni, Cu, □=Li vacancy) and **2** ternary transition metal nitrides of general formulation AMN_2 (A=alkaline earth metal, M=Ti, Zr, Hf). Compounds in class **1** are based on the hexagonal Li_3N structure, unique to nitrides. Compounds in group **2**, by contrast, crystallise with oxide structures (α-$NaFeO_2$ or $KCoO_2$). Specific and unusual synthetic methods have been developed to reproducibly prepare these compounds. Compounds in series **1** contain ordered or disordered Li vacancies at increased levels relative to the parent Li_3N, itself a Li^+ fast ion conductor. Nitrides in series **2** should be nominally diamagnetic ($S=0$), yet magnetic measurements reveal behaviour seemingly inconsistent with this assumption.

Keywords: Nitrides; Synthesis; Structure; Diffraction

1. Introduction

After several decades of dedicated research, advances in the chemistry of inorganic nitrides have accelerated dramatically over the last 5–10 years. Transition metal compounds illustrate many of the reasons why nitride chemistry is receiving increased attention. Exhibiting a particularly rich and unexpected valence behaviour, they already display evidence of both curious and useful electronic behaviour [1–3].

An emerging structural class within nitride chemistry are two dimensional, layered materials. Intriguing examples already exist within nominally simple binary systems such as A^I–N and A^{II}–N (A^I=Li, A^{II}=Ca, Sr, Ba). For example, Li_3N, crystallising with a unique layered structure [4,5], is the *only* stable alkali metal nitride. Also, Sr_2N and Ba_2N ('excess electron', *anti*-$CdCl_2$-type subnitrides) are the most stable nitrides of strontium and barium whereas 'Sr_3N_2' and 'Ba_3N_2' are ill-defined. Layered *ternary* nitrides broadly follow two patterns in terms of their crystal chemistry: those adopting structures with known analogues (chiefly from oxide chemistry) and those evolving from structures unique to nitrides (principally Li_3N or subnitride derivatives). In either case, knowledge of relatively well-characterised analogue or parent systems can be exploited to (a) establish a degree of structural predictability, (b) begin to modify and manipulate composition, structure and also, therefore physical properties of potential new materials.

Materials of stoichiometry ABX_2 are well-known in oxides and chalcogenides. The 2-D structural nature of many of these materials is intrinsic to their properties (e.g. batteries, electronic materials). Nitride ABX_2 examples now embrace alkali metal–transition metal and mixed transition metal systems. Alkaline earth metal compounds, however, are still relatively rare. ABN_2 nitrides are, in some cases, non-stoichiometric (e.g. $Li_{0.84}W_{1.16}N_2$) [6] with potential for (de)intercalation chemistry (e.g. $Li_{1-x}MoN_2$) [7]. Many of the studied materials are metallic and paramagnetic, whereas some show more unexpected and exciting behaviour (e.g. Ca_xTaN_2) [8].

By contrast, manipulation of the Li_3N parent structure via substitution of transition metals is not an entirely recent phenomenon. Originally, research into nominal $Li_{3-x}M_xN$ (M=Co, Ni, Cu) systems was performed over 50 years ago [9,10]. Solid solutions of limited range (typically $x<0.5$) were observed with retention of the Li_3N structure.

*Corresponding author.
E-mail address: Duncan.Gregory@Nottingham.ac.uk (D.H. Gregory).

0925-8388/01/$ – see front matter
PII: S0925-8388(00)01340-2

Substitution is ostensibly isovalent (M^+ for Li^+) on two-coordinate sites. Li_3N is a promising solid electrolyte with a performance inhibited only by its low decomposition potential. Recent work has focussed on the capability of substituted compounds as improved battery materials. The performance of such compounds might be tailored via increased stability and/or conductivity; the latter achieved through reduced activation energies and/or increased charge carrier concentration.

As part of continuing research into new layered nitride materials, we report here the systematic study of compounds within these two structural classes. $Li_{3-x-y}\square_yM_xN$ (M=Co, Ni, Cu, □=vacancy) nitrides have Li_3N-type structures containing either ordered or disordered Li^+ vacancies tuneable via choice of substituent and synthetic conditions. $A^{II}M^{IV}N_2$ nitrides (A=Sr, Ba; M=Ti, Zr, Hf) adopt structures with oxide analogues. The unexpected magnetic behaviour in these compounds has been investigated.

2. Experimental details

2.1. Starting materials

Binary starting materials, Li_3N, Sr_2N and Ba_2N were synthesised by the reaction of the molten alkaline earth metal–sodium alloys with dried nitrogen (at 650°C, 520°C and 520°C respectively). The cleaned metal (Alfa, 99+%) was added to molten sodium (Aldrich, 99.95%) in an Ar-filled glovebox and then heated in a stainless steel vessel under nitrogen for 48–72 h. Excess sodium was then removed by vacuum distillation at 350–400°C for 24 h. The identity of the powders was confirmed by powder X-ray diffraction (PXD) with negligible alkali or alkaline earth oxide impurities in the products.

2.2. $Li_{3-x-y}\square_yM_xN$ ternary nitride (series **1**) synthesis

Crystals of ternary nitrides were prepared by reaction of Li_3N with cleaned metal (M=Co, Ni, Cu) foil tubes (99.9%; 0.15 mm thickness). Foils were cleaned by reduction under 20% H_2/N_2 gas for 16 h at 600°C. This was essential to remove surface oxide. Reactions performed without the cleaning step produced predominantly Li_2O with no evidence of crystal growth. Tubes were placed inside a stainless-steel crucible, sealed in a stainless steel vessel under a positive N_2 pressure and heated to temperatures between 400 and 750°C for 5 days. Reactions yielded crystals in thick films on the surface of the foils varying in colour from silver/grey (cobalt) through gold and black (nickel) to dark blue (copper). The air-sensitive crystals were isolated and data collected either in sealed capillaries at 298 K or under RS3000 oil at 150 K ($Li_{1.78}Ni_{0.78}N$). Bulk nitrides were synthesised by reaction of Li_3N with reduced metal powders or with the binary transition metal nitrides (M_3N) at similar reaction temperatures (in 1:1 or higher ratios). M_3N starting materials were pre-synthesised via the action of dry NH_3 gas on metal halide powders at ca. 300° for 16 h. Both bulk and single crystalline products were highly sensitive to moist air.

2.3. $A^{II}M^{IV}N_2$ ternary nitride (series **2**) synthesis

Polycrystalline nitrides were prepared by the reaction of the binary alkaline earth nitrides with binary nitrides, TiN (Aldrich, 99%), ZrN (Johnson Matthey, 99%) or HfN (Aldrich, 99%) (1:1 ratios) [11–13]. All manipulations were performed in a purified Ar-filled glovebox. Pellets were wrapped in molybdenum foil and placed within stainless steel crucibles, which were subsequently welded closed under Ar. Crucibles were fired at 1000–1030°C for 5 days and cooled at 20°C/h to room temperature. No reaction of the nitrides with the interior of the Mo foil was observed. The reactions yielded powders of $SrTiN_2$ (black), $SrZrN_2$, $SrHfN_2$ (both dark gray/green), $BaZrN_2$ (deep red) and $BaHfN_2$ (orange/brown) respectively. Powders of solid solution members, $BaZr_{1-x}Hf_xN_2$ (x= 0.25, 0.5, 0.75) were prepared as above. $SrTiN_2$ was also prepared by reaction of the binary nitrides at 950°C in a purified N_2 atmosphere. Pellets (1:1 and 1:2 Sr_2N:TiN) were wrapped in Mo foil, placed within an alumina vessel and sealed. The vessel was evacuated, filled with purified N_2 gas and heated under N_2 for 2 days. $AZr(Hf)N_2$ nitrides hydrolyse rapidly in air (≤60 s) and violently with water, evolving ammonia. Reaction of $SrTiN_2$ with water is far less vigorous and samples remain black after several days of air exposure, but increase in volume. PXD of these samples shows the major phase to be $Sr(OH)_2$, with a poorly crystalline $SrTiN_2$-type phase still present.

2.4. Structure solution via single crystal X-ray diffraction

Single crystal diffraction data were collected for crystalline products of series **1**. Single crystal X-ray diffraction data were collected on a Stoe Stadi 4 four-circle diffractometer using graphite monochromated Mo Kα radiation. Structures were solved using SIR97 [14] and refined using SHELXL-93 [15]. All crystal structures in the Li/Cu/N system were solved in space group *P*6/*mmm* (analagous to Li_3N). Cu exclusively replaces Li in the interplanar position in $Li_{3-x}Cu_xN$ up to $x \approx 0.4$. The occupancy of the Li(1) site (0, 0, 1/2) was refined to approximately 0.4 Cu:0.6 Li in each case. The occupancy of the Li(2) site was left to vary freely. Little evidence of increased Li vacancies could be found within the Li_2N plane by X-ray diffraction for the majority of Li/Cu/N samples. However, the Li(2) site occupancy in crystals grown at 750°C refined

to 94(3)%[1]; 1–2% vacancies are present in the parent nitride, Li_3N. Further results of our investigations of crystal growth and structure with temperature in the Li/Cu/N system will be reported in due course [16].

Three compositions with different structures were identified in the the Li/Ni/N system: $Li_{1.78}Ni_{0.78}N$, LiNiN and $Li_5Ni_3N_3$. The first was solved in space group $P6/mmm$ with a refined Li(1) site occupancy of 0.22 Li:0.78 Ni and 78% Li occupying the Li(2) site[2]. The latter two compounds form structures with *ordered* Li vacancies. LiNiN crystallises in space group $P\bar{6}m2$ with a similar cell volume to Li_3N. $Li_5Ni_3N_3$ forms a supercell in space group $P\bar{6}2m$ with a ca. double that of the smaller $P6/mmm$ cell [17].

2.5. Bulk characterisation and structure determination

PXD data were collected using a Philips XPERT θ–2θ diffractometer with CuK_α radiation. Data for air-sensitive materials were collected using custom-designed sealed sample holders [18]. Cell parameters and phase purity were evaluated from short scans (ca. 1 h) over 5–80° 2θ using DICVOL91 [19] and IDENTIFY routines respectively.

Data were collected for the polycrystalline bulk products of series **1** from the same reactions that yielded single crystals and compared to single crystal structures. Data were also collected for bulk samples prepared via reaction of powdered starting materials. Crystalline 'bulk' products showed excellent agreement with diffraction patterns generated from single crystal data using POWDERCELL 2.3 [20]. Refined cell parameters were also in close agreement. Therefore we assume that the yield of crystals from each reaction were of essentially uniform composition. Bulk products prepared from powders yielded phases with very similar cell parameters but also generated small amounts of transiton metal impurity dependent on the initial ratio of Li:M.

All series **2** compounds contained levels of the respective alkaline earth metals and oxides as expected from the (nitrogen-weighted) starting ratios. The finely divided Sr and Ba metals are readily oxidised by low ppm oxygen. Zr- and Hf-nitride samples also contained either ZrN or HfN. $SrTiN_2$ prepared under N_2 from starting ratios of 1:2 Sr_2N:TiN contained unreacted TiN. Magnetic measurements were not performed on these latter samples. Diffraction data for Rietveld refinement were collected at approximately 298 K between 5 and 125° 2θ with step size 0.02° 2θ over ca. 15 h. Complete details of the structure determinations and refinements can be found elsewhere [11–13]. Impurity phases were simultaneously refined.

The morphology of the Li/Cu/N crystalline products in series **1** was evaluated by scanning electron microscopy (S.E.M.) using a Phillips XL 30 ESEM–FEG instrument running at either 10.0 or 15.0 kV in ultra high vacuum mode. Simultaneous energy dispersive analysis by X-rays (EDAX) was performed to determine the Cu:N ratio. Samples were loaded into the S.E.M. under a stream of N_2 gas to minimise reaction with air. Micrographs of the crystalline fragments show particles of hexagonal, platey or block-like habit of approximately 50–100 μm (Fig. 1). Spot scans over crystals yielded a Cu:N ratio of 0.4:1, in good agreement with the crystallographically determined stoichiometry.

Atomic absorption (AA) analysis for possible transition metal impurities in series **2** compounds, revealed only trace amounts of Fe, Cr and Ni ($\ll$1% by weight). The origin of these impurities is possibly from the steel crucibles or, more likely given the observed concentrations, from the MN starting materials. EDAX did not find any concentration of these elements within detectable limts. No phases of these transition metals were present in sufficient concentrations to be detectable by PXD.

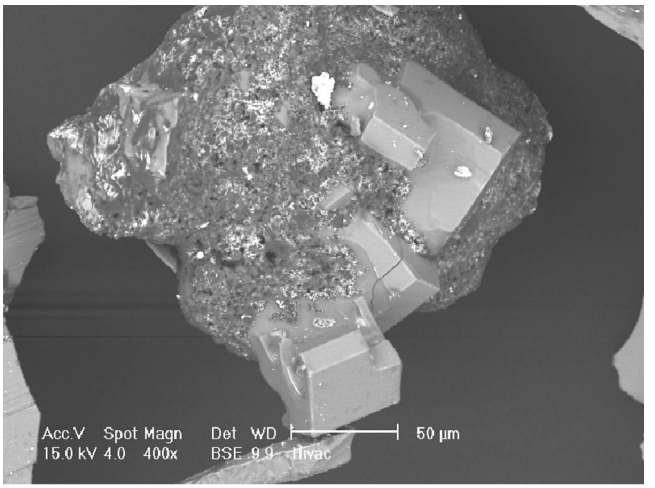

Fig. 1. S.E.M. micrograph of Li–Cu–N crystalline particles.

[1] $Li_{2.5}Cu_{0.4}N$: $M=56.77$. Hexagonal space group $P6/mmm$ (No. 191), $a=3.6808(3)$ Å, $c=3.7702(3)$ Å, $Z=1$, $V=44.236(6)$ Å^3, $\rho_{calc}=2.370$ g cm^{-3}. $\mu=5.91$ mm^{-1}. One hundred and sixty five reflections measured at 298(1) K, 28 independent ($R_{int}=0.0153$). Data collected on a Stadi-4 diffractometer with MoKα radiation $\lambda=0.71073$ Å. The structure was solved by direct methods with SIR97 and refined by least squares within SHELXL-93. $w=1/[\sigma^2(F_0^2)+(0.0000P)^2+0.0218P]$ where $P=(F_0^2+2F_c^2)/3$. $R1=0.0121$, $wR2=0.0281$.

[2] $Li_{1.78}Ni_{0.78}N$: $M=72.16$. Hexagonal space group $P6/mmm$ (No. 191), $a=3.7529(6)$ Å, $c=3.5309(9)$ Å, $Z=1$, $V=43.067(14)$ Å^3, $\rho_{calc}=3.782$ g cm^{-3}. $\mu=8.33$ mm^{-1}. One hundred and sixty five reflections measured at 150(1) K, 28 independent ($R_{int}=0.1155$). Data collected on a Stadi-4 diffractometer with MoKα radiation $\lambda=0.71073$ Å. The structure was solved by direct methods with SIR97 and refined by least squares within SHELXL-93. $w=1/[\sigma^2(F_0^2)+(0.0307P)^2+0.0000P]$ where $P=(F_0^2+2F_c^2)/3$. $R1=0.0288$, $wR2=0.0587$.

2.6. Magnetic measurements

Magnetic susceptibility measurements were performed on all series **2** AMN_2 samples (including $BaZr_{1-x}Hf_xN_2$ compositions) at 293 K using a Johnson Matthey balance. Calculated values were corrected for the measured diamagnetism of the sample tubes. Variable temperature magnetic measurements of AMN_2 compounds (ca. 0.3 g) were taken using a Cryogenic S100 SQUID susceptometer with a scan length of 3 cm to reduce field inhomogeneity to 0.5%. Data were collected between 5 K and room temperature, cooling first to 5 K at zero field and then subsequently warming under a field of 100 G. Measurements were taken at 2 K steps between approximately 5 and 100 K and at every 4 K between 100 and 298 K. Additional measurements over regions of specific interest were made with a smaller temperature step as necessary. The magnetic moment at each point was calculated from an average of four scans. Data were corrected for the diamagnetic contribution of the sample holders (either silica or gelatine capsules).

3. Results and discusssion

Single crystal and powder X-ray diffraction studies of series **1** compounds already reveal a host of phases and compositions within the Li–M–N systems. A summary of the structural information from single crystal diffraction is shown in Table 1. The structures of $Li_{3-x-y}M_{x-y}N$ phases are shown in Fig. 2. The Li–Cu–N system is seemingly the least flexible under the synthetic conditions employed. Only Li_3N-type structures were observed as both crystals and powders. Copper substitution is limited to levels approximating $x=0.4$ (higher than previously observed but lower than that achieved at high N_2 pressures [21]) and Li vacancies are disordered within the $[Li_2N]$ plane and low in concentration. The structure of the nitridocuprate, $Li_{2.5}Cu_{0.4}N$ is thus isotypic to Li_3N, with alternate layers of Li–N sheets and metal ions stacked perpendicular to the *c*-axis, with substituent Cu partially replacing Li at the Li(1) site located at the apices of N-centred hexagonal bipyramids, i.e. between Li–N planes. Possible generation of Li^+ vacancies in the $[Li_2N]$ (*ab*) plane is manifested in the increased *a* parameter relative to Li_3N.

Both disordered and ordered structures are seen in phases in the Li–Ni–N system. Common to these phases, and in contrast to the Li/Cu/N system, are relatively high levels of transition metal substitution between and vacancy inclusion within the $[Li_2N]$ planes. Consequently, whereas within the Li/Cu/N system metal substitution is close to isovalent and nitrogen coordination is almost unaffected, the contrary is true for M=Ni. As in the Li–Cu–N system, $Li_{1.78}Ni_{0.78}N$ forms a structure analogous to Li_3N (*P*6/*mmm*) with partial substitution of Ni on the interplanar Li(1) site and a disordered distribution of vacancies across the planar Li(2) site. Ordered variants also exist, however and unlike in their disordered counterparts, interplanar sites are fully occupied by the substituent transition metal (Ni). Li^+ vacancies within the $[Li_{2-y}N]$ plane occupy discrete sites, lowering the N coordination from 8 in Li_3N to '6+1' in $Li_5Ni_3N_3$ to 5 in LiNiN.

Our studies in the Li/Co/N system are not yet conclusive. Data from powders indicate that *P*6/*mmm* structures are obtained. Preliminary crystal growth experiments have produced small, platey particles that are difficult to isolate. We have yet to succeed in solving and refining structural data from crystals in this system and the obtained unit cells have thus far only been indexed in low symmetry (monoclinic) space groups.

As in Li_3N, Li within $[Li_{2-y}N]$ planes is coordinated to nitrogen in a trigonal planar arrangement in all cases. The Li–N bond lengths are consistently larger than those observed in the parent binary nitride. The interplane (Li,M)–N distances are considerably shorter than the equivalent Li(1)–N distance in Li_3N and are close in value to M–N bond distances in other nitrides where M is linearly coordinated (e.g. CaNiN: 1.7904 Å) [22]. Bond valence calculations [23] yield Li and N site valences slightly lower than Li_3N [24] and importantly the mag-

Table 1
Summary of structural parameters, bond lengths and bond valence sums (*V*) for $Li_{3-x-y}M_x\square_yN$ phases

Compound	Space group	*a*, *c*/Å	*x*	*y*	Li/M(1) site occupancy, Li:M	Li(2)–N/Å	Li/M(1)–N/Å	Nominal M^{n+} Ox. state	*V*: Li, (Li/M), N
$Li_{2.5}Cu_{0.4}N$	*P*6/*mmm*	3.6808(3), 3.7702(3)	0.4	0.12	0.6:0.4	2.1251(2)	1.8851(2)	1.3	0.8, 1.0, −2.5
$Li_{1.78}Ni_{0.78}N$[a]	*P*6/*mmm*	3.7529(6), 3.5309(9)	0.78	0.44	0.22:0.78	2.167(1)	1.765	1.6	0.7, 1.8, −2.8
$Li_5Ni_3N_3$	$P\bar{6}2m$	6.475(3), 3.555(2)	1	0.33	0:1	2.153(1)	1.777(1)	1.3	0.7, 1.9, −2.6
LiNiN	$P\bar{6}m2$	3.758(1), 3.540(1)	1	1	0:1	2.1697(1)	1.7700(5)	2.0	0.7, 1.9, −3.0
Li_3N [4]	*P*6/*mmm*	3.648(1), 3.8875(1)	0	0[b]	1:0	2.106	1.939	–	1.0, 0.8, −3.0

[a] Data collected at 150(1)K.
[b] Nominally, although ca. 0.02 experimentally.

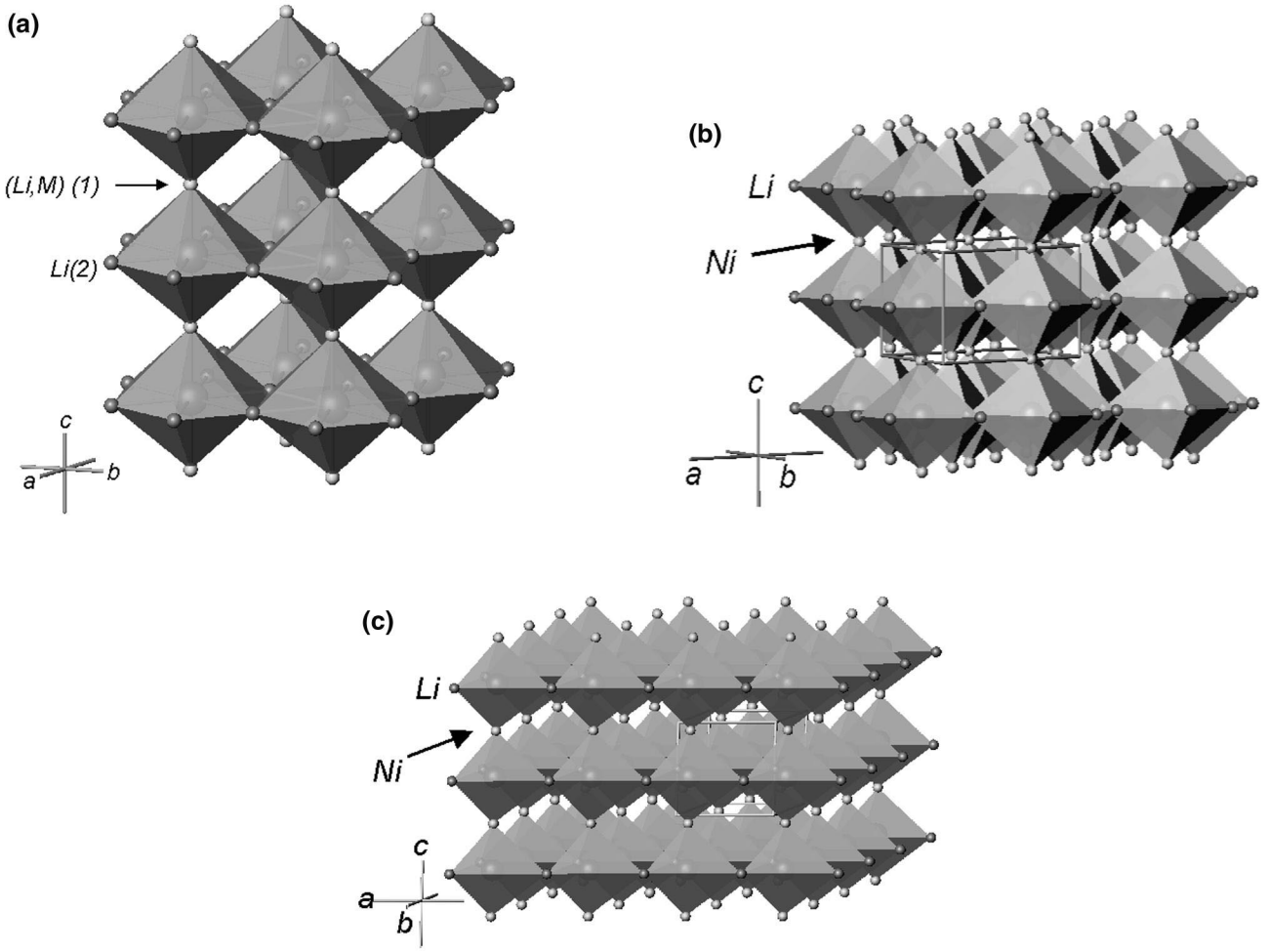

Fig. 2. Crystal structures of $Li_{3-x-y}M_x\square_yN$ phases: (a) disordered $P6/mmm$ (Li_3N-type) structure of $Li_{2.5}Cu_{0.4}N$ and $Li_{1.78}Ni_{0.78}N$; (b) ordered $P\bar{6}2m$ superstructure of $Li_5Ni_3N_3$; (c) ordered $P\bar{6}m2$ structure of LiNiN. Each structural representation shows N-centred polyhedra linked by vertices along *c* and by edges (Li_3N-type) or vertices (superstructures) in the *ab* plane.

nitude of the interplane (Li,M) site valence is increased relative to Li_3N. Although these values differ in quantitative terms from nominal oxidation states, the increases in the (Li,M) site valence and decreases in the Li site valence after metal substitution are further strong indicators that, in the Li/Ni/N system at least, substitution for lithium is not isovalent. An alternative interpretation might be additionally that the covalency of the (Li,M)–N bond increases with increasing substituent level, *x*. From the nominal oxidation states, creation of Li vacancies in the [Li_2N] plane is inevitable to maintain charge balance. The consequences of increased Li^+ vacancy levels (increased number of charge carriers) and increased (Li,M)–N covalent bond character (reduced activation energies) might be significant with respect to ionic conductivity.

PXD results of series **2** compounds show that two structure types so far exist in the ternary alkaline earth-group IV nitrides (Fig. 3). $SrTiN_2$ and $BaMN_2$ (M=Zr, Hf) crystallise with the $KCoO_2$ structure in tetragonal space group $P4/nmm$ (No. 129). A continuous solid solution, $BaZr_{1-x}Hf_xN_2$ ($0 \le x \le 1$), also exists with retention of the $KCoO_2$ structure. $SrMN_2$ (M=Zr, Hf) crystallise with the α-$NaFeO_2$ structure in hexagonal space group $R3m$ (No. 166). The structure of $BaZrN_2$, although previously reported [25], was refined here, to allow (a) a comparison with the published structure and (b) quantitative analysis of impurity phases, essential for interpreting the magnetic measurements. A summary of the key features is presented in Table 2. Important interatomic distances and calculated bond valence sums are shown in Table 3.

Room temperature (293 K) magnetic measurements of all samples yielded mass susceptibility values indicative of paramagnetic materials ($SrZrN_2$, $SrHfN_2$: $\chi_g = 3.39 \times 10^{-6}$ and 1.71×10^{-7} emu g^{-1} respectively. $SrTiN_2$: $\chi_g = 5.28 \times 10^{-5}$ emu g^{-1}. All Ba(Zr,Hf)N_2 samples gave χ_g values of ca. 3×10^{-5} emu g^{-1}, tending to increase slightly with Hf content at room temperature. $AZrN_2$ and $AHfN_2$ samples show weak, temperature independent paramagnetism between ca. 10–300 K with superconducting transitions below 10 K. Critical temperature (T_c) onsets are at ca. 9.5, 8.9, 9.9 and 8.9 K for $BaZrN_2$, $BaHfN_2$, $SrZrN_2$

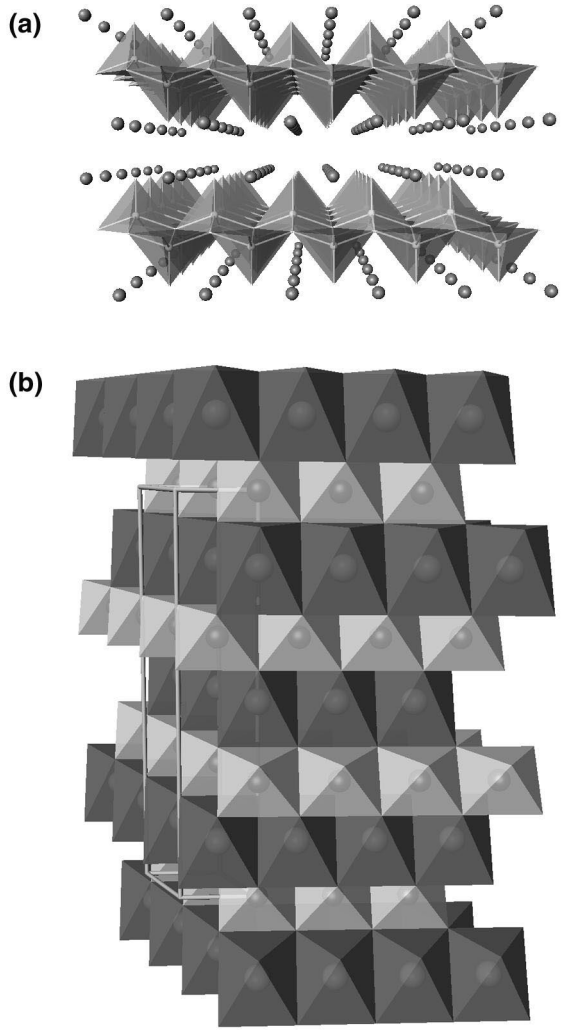

Fig. 3. Crystal structures of $A^{II}M^{IV}N_2$ compounds: (a) $KCoO_2$-type structure of $SrTiN_2$, $Ba(Zr,Hf)N_2$, showing layers of edge-sharing MN_5 square-based pyramids separated by A atoms; (b) α-$NaFeO_2$-type structure of $SrZr(Hf)N_2$ showing alternating edge-sharing layers of AN_6 (dark grey) and MN_6 octahedra (light grey).

and $SrHfN_2$, respectively (Fig. 4). Magnetic measurements of $SrTiN_2$ show no superconducting transition above 4 K. Between ca. 40–300 K, samples exhibit temperature dependent paramagnetism. Ca. 80% of $SrTiN_2$ samples synthesised show a sharp drop in susceptibility at ca. 41.5 K, possibly indicative of antiferromagnetic ordering or spin glass behaviour. Further measurements of $SrTiN_2$ samples are in progress.

The two structure types of the group IV ternary nitrides both contain M–N layers between which are located alkaline earth cations. The structures differ in the coordination of the transition metals in these layers. $SrZr(Hf)N_2$ adopt the α-$NaFeO_2$ structure in which layers of edge-sharing MN_6 octahedra are separated by layers of octahedrally coordinated Sr^{2+} cations. $Ba(Zr,Hf)N_2$ and $SrTiN_2$ adopt the much rarer $KCoO_2$ structure. Here Ba^{2+} or Sr^{2+} sit between layers of edge-sharing $[MN_2]^{2-}$ square pyramidal anions. The mean Zr(Hf)–N distances are of the same *order* in both structure types, although the distances (notably the M–N apical distance) are slightly shorter in the $KCoO_2$ structure types. This suggests a greater covalent contribution to the transition metal–nitrogen bonding in these structures and this is reflected in the high bond valence sums observed. Similar short M–N distances (and specifically again, the apical M–N distance) are seen in $SrTiN_2$. The mean Sr–N distance in $SrTiN_2$ is ~0.1 Å longer than that in the α-$NaFeO_2$ types structures yielding a bond valence sum of comparable value to that seen in the sub-nitride, Sr_2N. The bond lengths observed for $BaZrN_2$ are consistent with the previous study [25].

The coordination of the alkaline earth atoms mirrors that of the transition metals in both structure types, octahedral in $SrZr(Hf)N_2$ and square pyramidal in $BaZr(Hf)N_2$ and $SrTiN_2$. Nitrogen coordination is distorted octahedral in the α-$NaFeO_2$ type structures and both distorted octahedral and tetrahedral in the $KCoO_2$ isotypes. The formation of AMX_2 structure-types in oxide and chalcogenide chemistry has been extensively studied and related to factors such as ion size and ionicity [26]. With the number of known AMN_2 structures steadily increasing, it may soon be possible to categorise nitrides in a similar manner. Preliminary studies of other group IV and V transition metal AMN_2 nitride systems indicate other structure-types also exist.

The magnetic data for Zr- and Hf-containing samples are not consistent with diamagnetic $S=0$, $d=0$ species

Table 2
Summary of crystallographic features/indices for AMN_2 phases

Nitride	Space group	a/Å	c/Å	c/a	R_{wp}	R_p	R_e	R_I
$SrTiN_2$	$P4/nmm$	3.8799(2)	7.6985(4)	1.98	0.085	0.065	0.013	0.036
$BaZrN_2$	$P4/nmm$	4.1620(1)	8.3848(2)	2.01	0.087	0.065	0.011	0.019
$BaHfN_2$	$P4/nmm$	4.1279(1)	8.3816(4)	2.03	0.104	0.078	0.009	0.025
$SrZrN_2$	$R\bar{3}m$	3.3730(1)	17.6756(3)	5.24	0.073	0.054	0.014	0.011
$SrHfN_2$	$R\bar{3}m$	3.3448(1)	17.6779(2)	5.29	0.076	0.051	0.007	0.019
$BaZr_{0.25}Hf_{0.75}N_2$	$P4/nmm$	4.136(2)	8.389(4)	2.03	–	–	–	–
$BaZr_{0.5}Hf_{0.5}N_2$	$P4/nmm$	4.141(3)	8.379(8)	2.02	–	–	–	–
$BaZr_{0.75}Hf_{0.25}N_2$	$P4/nmm$	4.1498(1)	8.3843(4)	2.02	–	–	–	–

Table 3
Important interatomic distances and site valences (V) for AMN_2 phases

Nitride	A–N/Å	M–N/Å	M–M/Å	V(A)	V(M)	V(N)
$SrTiN_2$	2.581(7)×1, 2.7445(2)×4	1.839(7)×1, 2.056(1)×4	3.063(1)×4	1.4	4.1	2.8, 2.7
$BaZrN_2$	2.67(1)×1, 2.9449(7)×4	2.06(1)×1, 2.2072(7)×4	3.290(1)×4	1.7	4.2	3.1, 2.9
$BaHfN_2$	2.68(2)×1, 2.922(1)×4	2.05(2)×1, 2.1856(5)×4	3.254(1)×4	1.8	4.2	3.1, 2.9
$SrZrN_2$	2.609(3)×6	2.292(2)×6	3.373(1)×6	2.2	3.7	2.9
$SrHfN_2$	2.602(3)×6	2.273(2)×6	3.344(1)×6	2.2	3.7	2.9

suggested by the nominal stoichiometry, AMN_2. The most likely explanation for this apparent anomally are MN impurities which are paramagnetic between approximately 10–300 K and have superconducting transitions near 10 K; ZrN at 10.0 K and HfN at 8.83 K [27]. We are continuing to develop the synthetic methodology to allow us to obtain ternary nitrides containing minimal levels of impurities. The magnetic data for $SrTiN_2$ also seem anomalous for a nominal $S=0$, $d=0$ compound. At present, however, we have no adequate explanation for the observed magnetism in the nitridotitanate. Unlike $AZr(Hf)N_2$ samples, there is no evidence for the binary MN nitride in $SrTiN_2$ samples. TiN is a superconductor below ca. 6.5 K (as measurements have confirmed on samples of our starting material) and we do not observe this transition. Only trace amounts of other transition metal impurities are present. We are now extending our magnetic and structural studies of this system.

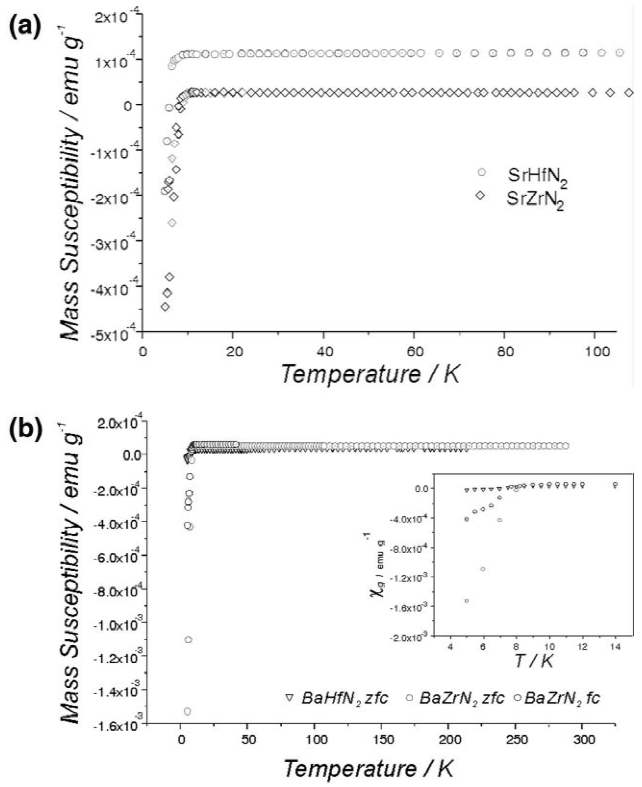

Fig. 4. Plots of mass magnetic susceptibility vs. temperature for (a) $SrZr(Hf)N_2$, (b) $BaZr(Hf)N_2$.

4. Conclusions

In summary, we have prepared new ternary transiton metal nitrides within two broad structural classes of layered compounds. Studies of lithium late transiton metal nitrides continue to generate new phases derived from the α-Li_3N structure-type. Crystals can be reproducibly grown from reaction of Li_3N at transition metal surfaces. Higher levels of transition metals than previously reported have been substituted at ambient pressure using this methodology and the Li_3N derivatives so produced contain Li^+ vacancies with concentrations and distributions dependent on the substituent metal and synthetic conditions. The nominal transition metal oxidation state varies in accordance with the vacancy concentration, y. The impact of these enhanced vacancy levels on electronic properties is under investigation.

To date, we have observed two layered structure types adopted by $A^{II}M^{IV}N_2$ compounds, differing principally in the coordination of the transition metal within layers. Bond lengths in the $KCoO_2$-type series of compounds indicate significant covalent (π-type) bonding contributions between transition metals and nitrogen. Magnetic investigations reveal behaviour unexpected for nominal $S=0$ compounds. While this may be rationalised in terms of binary nitride impurities in M=Zr, Hf samples, further investigations might reveal whether the observed properties are intrinsic to any of the ternary nitrides themselves.

Acknowledgements

The authors thank Dr M. Slaski for magnetic measurements and Dr D.P. Weston for assistance with SEM/EDAX. D.H.G. thanks the EPSRC for the award of an Advanced Fellowship and for funding this work. The authors also acknowledge the University of Nottingham for studentships for P.M.O., A.G.G. and D.J.S.

References

[1] D.H. Gregory, J. Chem. Soc. Dalton Trans. (1999) 259.
[2] R. Niewa, F.J. DiSalvo, Chem. Mater. 10 (1998) 2733.
[3] S. Yamanaka, K. Hotehama, H. Kawaji, Nature 392 (1998) 580.
[4] A. Rabenau, H. Schultz, J. Less-Common Met. 50 (1976) 155.
[5] H. Schultz, K.H. Thiemann, Acta Crystallogr., Sect. A 35 (1979) 309.
[6] S. Kaskel, D. Hohlwein, J. Strähle, J. Solid State Chem. 138 (1998) 154.
[7] S.H. Elder, L.H. Doerrer, F.J. DiSalvo, J.B. Parise, D. Guyomard, J.M. Tarascon, Chem. Mater. 4 (1992) 928.
[8] V. Balbarin, R.B. Van Dover, F.J. DiSalvo, J. Phys. Chem. Solids 57 (1996) 1919.
[9] W. Sachsze, R. Juza, Z. Anorg. Allg. Chem. 259 (1949) 278.
[10] R. Juza, K. Langer, K. von Benda, Angew. Chem. 80 (1968) 373; R. Juza, K. Langer, K. von Benda, Angew. Chem. Int. Ed. Engl. 7 (1968) 360.
[11] D.H. Gregory, M.G. Barker, P.P. Edwards, M. Slaski, D.J. Siddons, J. Solid State Chem. 137 (1998) 62.
[12] D.H. Gregory, M.G. Barker, P.P. Edwards, D.J. Siddons, Inorg. Chem. 35 (1996) 7608.
[13] D.H. Gregory, M.G. Barker, P.P. Edwards, D.J. Siddons, Inorg. Chem. 37 (1998) 3775.
[14] A. Altomare, M.C. Burla, M. Camalli, G.L. Cascarano, C. Giacovazzo, A. Guagliardi, A.G.G. Moliterni, G. Polidori, R. Spagna, J. Appl. Crystallogr. 32 (1999) 115.
[15] G.M. Sheldrick, SHELXL-93. Program for Crystal Structure Refinement, University of Gottingen, Gottingen, Germany, 1993.
[16] A.G. Gordon, A.J. Blake, D.P. Weston, D.H. Gregory, in preparation.
[17] M.G. Barker, A.J. Blake, P.P. Edwards, D.H. Gregory, T.A. Hamor, D.J. Siddons, S.E. Smith, J. Chem. Soc. Chem. Commun. (1999) 1187.
[18] M.G. Barker, M.J. Begley, P.P. Edwards, D.H. Gregory, S.E, Smith, J. Chem. Soc. Dalton Trans. (1996) 1.
[19] A. Boultif, D. Louer, J. Appl. Cryst. 24 (1991) 987.
[20] G. Nolze, W. Kraus, Powder Diffraction 13 (1998) 256.
[21] M.T. Weller, S.E. Dann, P.F. Henry, D.B. Currie, J. Mater. Chem. 9 (1999) 283.
[22] M.Y. Chern, F.J. DiSalvo, J. Solid State Chem. 88 (1990) 459.
[23] N.E. Brese, M. O'Keeffe, Acta Crystallogr., Sect. B 47 (1991) 192.
[24] N.E. Brese, M. O'Keeffe, Struct. Bonding (Berlin) 79 (1992) 307.
[25] O. Seeger, M. Hoffmann, J. Strähle, J.P. Laval, B. Frit, Z. Anorg. Allg. Chem. 620 (1994) 2008.
[26] C. Delmas, J.-J. Braconnier, C. Fouassier, P. Hagenmuller, Z. Naturforsch. 36b (1981) 1368.
[27] L.E. Toth, Transition Metal Carbides and Nitrides, Academic Press, New York, 1971.